Freedericksz instability for the twisted nematic device: A three-dimensional analysis

G. I. Sfyris,[1] K. Danas,[1] G. Wen,[1] and N. Triantafyllidis[1,2]
[1]*LMS, Ecole Polytechnique, CNRS, Université Paris-Saclay, 91128 Palaiseau, France*
[2]*Aerospace Engineering Department & Mechanical Engineering Department, The University of Michigan, Ann Arbor, Michigan 48109-2140, USA*
(Received 18 September 2015; published 27 July 2016)

Of interest here is the fully three-dimensional analysis of the Freedericksz transition for the twisted nematic device (TND), which is widely used in liquid-crystal display monitors. Using a coupled electromechanical variational formulation, the problem is treated as a bifurcation instability triggered by an externally applied electric field. More specifically, we study a finite thickness liquid-crystal layer, anchored between two infinite parallel plates relatively rotated with respect to each other by a given twist angle and subjected to a uniform electric field perpendicular to these bounding plates. The novelty of the proposed analysis lies in the fully three-dimensional formulation of the TND problem that considers all possible bounded perturbations about the principal solution. By scanning a wide range of the liquid crystal's material parameter space, we establish whether the Freedericksz transition is *global*, i.e., has an eigenmode depending solely on the layer thickness coordinate, or *local* (also termed the periodic Freedericksz transition), i.e., has an eigenmode with finite wavelengths in one or both directions parallel to the plate. It is found that global modes are typical for low values, while local modes appear at large values of the twist angle. Moreover, for certain TND's, the increase in twist angle can lower the critical electric field, findings that could be useful in guiding liquid-crystal selection for applications.

DOI: 10.1103/PhysRevE.94.012704

I. INTRODUCTION

Nematic continua are materials with elongated rodlike molecules that have preferred local average directions, which are modeled as directors. These materials exhibit important multiphysics coupling properties between their director orientation and externally applied mechanical, electric, magnetic, or thermal fields. In addition to their theoretical interest, they are of tremendous importance to applications, particularly in the form of liquid crystals, which have revolutionized the display technology in the form of liquid-crystal displays (LCDs). The twisted nematic device (TND) is the most widely used fundamental building block of LCDs, and it is the object of the present investigation.

The TND consists of a liquid-crystal layer anchored between two parallel plates. One of the plates is rotated with respect to the other by an angle $\Delta\phi$: 90° for a typical TND or 270° for a supertwisted nematic device (STND). In the absence of a transverse (i.e., normal to the bounding plates) electric field, all the directors are parallel to the bounding plates and form helices that rotate the light by $\Delta\phi$, allowing its passing through the two polarized end plates (their polarization directions differ by $\Delta\phi$). When the applied transverse electric field exceeds a critical value, the directors suddenly acquire a transverse component. This phenomenon, termed the *Freedericksz transition*, is responsible for the change of polarization direction in the light, which prevents its passage through the device.

The Freedericksz transition was discovered in the late 1920s [1,2], while its TND version—which opened the door for the display technology revolution due to its low transition voltage—was discovered in the 1970s [3]. The discovery of the STND [4] followed, and since then developments in this field have progressed exponentially (see, e.g., [5]). On the theoretical side, the continuum mechanics modeling of the free energy for liquid crystals using a unit vector termed the *director* to represent the local macromolecular orientation was introduced in [6–8], while the full theory for the time-dependent behavior of these materials was subsequently introduced in [9,10] (for a more recent general continuum theory, see also [11]).

The present work is motivated by the fact that modeling the Freedericksz transition problem in the liquid-crystal literature (see, for example, the standard excellent textbooks [12,13]), is often based on a one-dimensional (1D) analysis that uses director fields depending solely on the layer thickness coordinate (see, e.g., more recent work [14,15]). Special cases that require 2D considerations have been shown to exist [16] (see also the book by Virga [17] for more details) exhibiting finite (with respect to the plate-parallel coordinates) wavelength eigenmodes, termed *periodic Freedericksz transitions*.

For problems involving Freedericksz transitions in TNDs, perturbation methods involving 1D or 2D approximations for the director field are frequently used (e.g., see [18–20]) for the sake of analytical tractability. However, no systematic, general investigation of the Freedericksz transition problem for the TND has been presented, to the best of our knowledge, that considers all possible eigenmodes in order to select the critical one (corresponding to the lowest electric field) and to thus establish whether this mode is *global*, i.e., dependent solely on the thickness coordinate (and thus captured by a 1D analysis) or *local*, i.e., has finite wavelengths with respect to one or both in-plane coordinate directions (and thus requiring a full 3D modeling).

The Freedericksz transition in a fully anchored TND is modeled here as a bifurcation problem for the finite-thickness liquid crystal with a Frank-Oseen energy, where the loading parameter is the magnitude of the applied transverse electric field. The continuum mechanics model uses a novel coupled electromechanical variational principle for nematic elastomers proposed by [21], where the Euler-Lagrange equations are the mechanical equilibrium equations plus the Faraday law for

the electric field. A remark is in order at this point about our choice of the Frank-Oseen energy density for this work: experiments in liquid crystals found the Frank-Oseen model to be an adequate description of their energy density [22–24], while the most efficient materials for the TND are MBBA [25] and 5CB [26], with the parameters for the latter case serving as the base case for our calculations.

The work is organized as follows: after the introduction in Sec. I, we present in Sec. II a theoretical analysis of the fully three-dimensional boundary-value problem for the electromechanically coupled TND. This section is divided into four subsections. Section II A gives the energy functional based on the Frank-Oseen constitutive law and a quadratic polarization energy. In Sec. II B, we present the principal solution and derive the Euler-Lagrange equations and the associated natural boundary conditions. The critical point on the principal solution, i.e., the lowest electric-field strength and the corresponding eigenmode, are given in Sec. II C. The nondimensionalization of the problem parameters and the coefficients of the Euler-Lagrange equations appear in Sec. II D.

Next appear the results in Sec. III, which is divided into three subsections. In Sec. III A, we derive the analytical solution for the fully 3D boundary-value problem of a nematic liquid crystal for zero twist; this solution is used to compare our results with the existing literature on periodic Freedericksz transitions and as a highly nontrivial check for the numerical algorithm developed for the general case. For arbitrary values of the TND twist angle, no analytical solution can be found, and a mixed analytical and numerical technique, combining a finite-element discretization for the thickness coordinate with a Fourier transform for the remaining coordinates, is presented in Sec. III B to solve the bifurcation problem at hand. The results of our simulations are presented in Sec. III C. By scanning a wide range of the liquid crystal's material parameter space for different values of the twist angle, we establish whether the Freedericksz transition corresponds to a global or a local mode, and we find the critical electric field and the corresponding wave numbers. Finally, the main conclusions of our study are discussed in Sec. IV.

II. THEORY

In this section, we present the fully 3D boundary-value problem for the TND under full anchoring boundary conditions, using the coupled electromechanical variational formulation introduced by [21]. Based on the system's energy functional, we calculate its second functional derivative on the principal solution and subsequently derive the Euler-Lagrange equations and associated natural boundary conditions, governing the eigenvalue problem at the bifurcation point. Finally, we introduce a set of dimensionless variables to simplify the presentation of our results.

A. Energy functional

We consider a three-dimensional (3D) nematic-liquid-crystal layer, of density ρ, which is infinite in the x_1 and x_2 directions while it is confined in the x_3 direction by two parallel plates at distance ℓ, as seen in Fig. 1. The top plate is rotated by

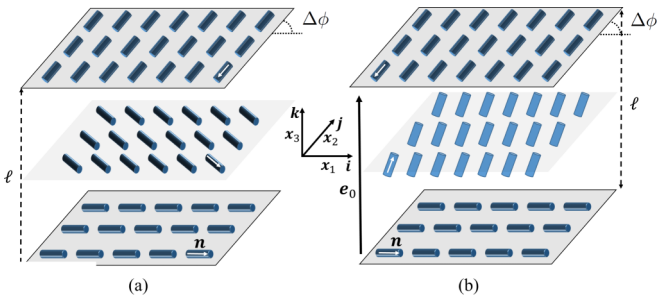

FIG. 1. A typical twisted nematic device with a 90° twist angle. In (a) the strength of the electric field is below its critical value and the nematic molecules in each $x_3 = \text{const}$ plane are parallel to the bounding plates, while in (b) the strength of the electric field is above its critical value and the molecules in each $x_3 = \text{const}$ plane rotate out of their plane, tending to align with the externally applied electric field.

an angle $\Delta\phi$ with respect to the bottom plate, thus introducing a twist $\tau \equiv \Delta\phi/\ell$. Usually in applications $\Delta\phi = \pi/2$, although higher angles are also encountered (supertwisted devices, $\Delta\phi = 7\pi/3$ or $3\pi/2$, e.g., see [4]).

The free energy, ψ, per unit volume of an incompressible nematic liquid crystal can be modeled as the sum of two contributions (see [21]): the Frank-Oseen (FO) energy ψ^{FO} of a cholesteric liquid crystal, and a polarization energy ψ^{P} that is caused by the electric field:

$$\psi(\mathbf{n},\mathbf{n}\nabla,\mathbf{p}) = \psi^{\text{FO}}(\mathbf{n},\mathbf{p}) + \psi^{P}(\mathbf{n},\mathbf{p}), \tag{1}$$

where

$$\psi^{\text{FO}} = \tfrac{1}{2}k_1(\nabla\cdot\mathbf{n})^2 + \tfrac{1}{2}k_2[\mathbf{n}\cdot(\nabla\times\mathbf{n}) + \tau]^2 + \tfrac{1}{2}k_3||\mathbf{n}\times(\nabla\times\mathbf{n})||^2, \tag{2}$$

$$\psi^{P} = \frac{1}{2\varepsilon_0}\left[\chi^{-1}(\mathbf{p}\cdot\mathbf{p}) + \left(\chi_n^{-1} - \chi^{-1}\right)(\mathbf{p}\cdot\mathbf{n})^2\right], \tag{3}$$

where k_1, k_2, and k_3 are positive constants [27], called in the literature the *splay*, *twist*, and *bend* constants, respectively, of the Frank-Oseen model, and τ is the twist of the unloaded system (i.e., prior to the application of an electric field). In (3), $\mathbf{p}$ is the polarization vector while χ and χ_n are the electric susceptibility constants in directions parallel and perpendicular, respectively, to the director vector $\mathbf{n}$, and ε_0 is the electric permittivity of the free space.

The system's total electric field $\mathbf{e}$ is the sum of the externally applied electric field in the absence of the liquid crystal $\mathbf{e}_0$ plus a perturbation $\widehat{\mathbf{e}}$, due to the presence of the polarizable liquid crystal (e.g., see [28]):

$$\mathbf{e} = \mathbf{e}_0 + \widehat{\mathbf{e}}. \tag{4}$$

The total (perturbed) electric displacement $\mathbf{d}$ ($\widehat{\mathbf{d}}$) is connected to the polarization $\mathbf{p}$ and the above-defined total (perturbed) electric field $\mathbf{e}$ ($\widehat{\mathbf{e}}$) by

$$\mathbf{d} = \mathbf{d}_0 + \widehat{\mathbf{d}} = \varepsilon_0\mathbf{e} + \mathbf{p};\ (\mathbf{d}_0 = \varepsilon_0\mathbf{e}_0,\ \widehat{\mathbf{d}} = \varepsilon_0\widehat{\mathbf{e}} + \mathbf{p}). \tag{5}$$

Due to the absence of free electric charges,

$$\nabla\cdot\mathbf{d} = \mathbf{0};\ (\nabla\cdot\widehat{\mathbf{d}} = \mathbf{0}), \tag{6}$$

we introduce a vector potential $\boldsymbol{\alpha}$ connected to the perturbed electric displacement $\widehat{\mathbf{d}}$ by

$$\widehat{\mathbf{d}} = \nabla \times \boldsymbol{\alpha}. \tag{7}$$

In addition to the liquid crystal's free-energy density ψ defined in (1), the system's electric energy density ψ^e needs to be added:

$$\psi^e = \tfrac{1}{2}\varepsilon_0 \mathbf{e}\cdot\mathbf{e}. \tag{8}$$

In view of the absence of an electric field outside the two bounding planes of the TND, the system's total potential energy $\mathcal{P}$ is the integral over the domain $V \equiv \mathbb{R}\times[-\ell/2,\ell/2]$ of the energy densities defined in (1) and (8) and takes the form (for derivation details, see [21])

$$\begin{aligned}\mathcal{P} = \int_V \Big[&\frac{1}{2}[k_1(\nabla\cdot\mathbf{n})^2 + k_2[\mathbf{n}\cdot(\nabla\times\mathbf{n}) + \tau]^2 \\ &+ k_3||\mathbf{n}\times(\nabla\times\mathbf{n})||^2] \\ &+ \frac{1}{2\varepsilon_0}\big[\chi^{-1}(\mathbf{p}\cdot\mathbf{p}) + \big(\chi_n^{-1}-\chi^{-1}\big)(\mathbf{p}\cdot\mathbf{n})^2 \\ &+ ||\nabla\times\boldsymbol{\alpha}-\mathbf{p}||^2\big] - \mathbf{e}_0\cdot\mathbf{p} \\ &+ \frac{k}{2\ell^2\xi_1}(\mathbf{n}\cdot\mathbf{n}-1)^2 + \frac{1}{2\varepsilon_0\xi_2}(\nabla\cdot\boldsymbol{\alpha})^2\Big] dV. \end{aligned} \tag{9}$$

The last two terms in the integrand of $\mathcal{P}$ are penalty terms, where the small dimensionless positive constants $(0<\xi_1,\xi_2<<1)$ are associated with the problem's two constraints: (i) the fact that the director $\mathbf{n}$ is a unit vector, i.e., $||\mathbf{n}||=1$, and (ii) the need for a unique potential $\boldsymbol{\alpha}$ in (7), which is hereby imposed by the Coulomb gauge $\nabla\cdot\boldsymbol{\alpha}=\mathbf{0}$. We have adopted a penalty formulation of these constraints in view of the numerical solution algorithm that is subsequently discussed. The parameter k used for the definition of the dimensionless penalty term ξ_1 is a convenient norm of the Frank-Oseen constants [to be defined in (22)].

At the interfaces between the bounding plates and the liquid crystal, we assume strongly anchoring (essential) boundary conditions for the director $\mathbf{n}$, namely

$$\begin{aligned}\mathbf{n}(x_1,x_2,-\ell/2) &= (\cos(\Delta\phi/2), -\sin(\Delta\phi/2),0),\\ \mathbf{n}(x_1,x_2,+\ell/2) &= (\cos(\Delta\phi/2), \sin(\Delta\phi/2),0).\end{aligned} \tag{10}$$

The equilibrium solutions for the TND are found by minimizing the system's potential energy $\mathcal{P}(\mathbf{n},\mathbf{p},\boldsymbol{\alpha})$ in (9) subject to the essential boundary conditions for $\mathbf{n}$ in (10). No boundary constraints are imposed on $\boldsymbol{\alpha}$ since the corresponding natural boundary conditions ($\mathbf{k}\times\widehat{\mathbf{e}}=\mathbf{0}$) are compatible with the fixed electric potential (voltage) difference between the two end plates.

B. Principal solution

The equilibrium for the twisted nematic device is given by the minimization of $\mathcal{P}$, i.e., the vanishing of the first variation of the potential energy:

$$\mathcal{P}_{,\mathbf{v}}(\mathbf{v})\delta\mathbf{v} = \mathbf{0}, \quad \mathbf{v}\equiv(\mathbf{n},\mathbf{p},\boldsymbol{\alpha}). \tag{11}$$

An external transverse electric field (i.e., along the x_3 direction, as shown in Fig. 1) is applied perpendicular to the bounding plates with magnitude e_0. For as long as the strength of the applied electric field is below a critical value (the sought-after Freedericksz transition value e_0^c), all directors $\mathbf{n}$ remain at their initial position. The obvious solution to the above equation is termed the *principal solution* recorded below, where all associated field quantities are denoted by a superscript 0:

$$\overset{0}{\mathbf{v}} = \begin{cases} \overset{0}{\mathbf{n}} = (\cos(\tau x_3), \sin(\tau x_3), 0),\\ \overset{0}{\mathbf{p}} = (0,0,\varepsilon_0 e_0\chi/(1+\chi)),\\ \overset{0}{\boldsymbol{\alpha}} = (0,0,0).\end{cases} \tag{12}$$

The principal solution for the director vector is the initial uniform helix of the nematic device about the x_3 axis, where all directors lie in planes parallel to the end plates ($\overset{0}{n}_3 = 0$), as seen in Fig. 1(a). Notice that the polarization vector for that solution has only an x_3 component.

C. Critical electric field on the principal solution and the corresponding eigenmode

At small values of the externally applied electric field, the principal solution $\overset{0}{\mathbf{v}}$ is stable since it is a local minimizer of the energy; further increase in the electric field strength, and specifically above a *critical value* e_0^c, results in the principal solution no longer being a minimizer of the potential energy. A new bifurcated equilibrium solution emerges at e_0^c, as can be seen in Fig. 1(b). This bifurcation phenomenon is called the *Freedericksz transition*.

The bifurcation condition, occurring at e_0^c along a particular direction $\Delta\mathbf{v}$, called the *critical mode*, is found by the vanishing of the second functional derivative of $\mathcal{P}$ evaluated on the principal solution, namely

$$\begin{aligned}\Big(\mathcal{P}_{,\mathbf{vv}}\Big(\overset{0}{\mathbf{v}}(e_0^c),e_0^c\Big)\Delta\mathbf{v}\Big)\delta\mathbf{v} = 0; \quad \Delta\mathbf{v}\equiv(\Delta\mathbf{n},\Delta\mathbf{p},\Delta\boldsymbol{\alpha}),\\ \delta\mathbf{v}\equiv(\delta\mathbf{n},\delta\mathbf{p},\delta\boldsymbol{\alpha}),\end{aligned} \tag{13}$$

where $\Delta\mathbf{v}$ is the bifurcation eigenmode, and $\delta\mathbf{v}$ denotes the arbitrary test functions corresponding to the problem's independent variables $\mathbf{v}$.

The above equation takes, in view of (9), the following explicit form:

$$\begin{aligned}(\mathcal{P}^0_{,\mathbf{vv}}\Delta\mathbf{v})\delta\mathbf{v} = \int_V \Big(&k_1(\nabla\cdot\Delta\mathbf{n})(\nabla\cdot\delta\mathbf{n}) + \frac{k}{\ell^2\xi_1}\Big(\Delta\mathbf{n}\cdot\overset{0}{\mathbf{n}}\Big)\Big(\delta\mathbf{n}\cdot\overset{0}{\mathbf{n}}\Big)\\ &+ k_2\Big[\Delta\mathbf{n}\cdot\Big(\nabla\times\overset{0}{\mathbf{n}}\Big) + \overset{0}{\mathbf{n}}\cdot(\nabla\times\Delta\mathbf{n})\Big]\Big[\delta\mathbf{n}\cdot\Big(\nabla\times\overset{0}{\mathbf{n}}\Big) + \overset{0}{\mathbf{n}}\cdot(\nabla\times\delta\mathbf{n})\Big]\\ &+ k_3\Big[\Delta\mathbf{n}\times\Big(\nabla\times\overset{0}{\mathbf{n}}\Big) + \overset{0}{\mathbf{n}}\times(\nabla\times\Delta\mathbf{n})\Big]\cdot\Big[\delta\mathbf{n}\times\Big(\nabla\times\overset{0}{\mathbf{n}}\Big) + \overset{0}{\mathbf{n}}\times(\nabla\times\delta\mathbf{n})\Big]\end{aligned}$$

$$+\frac{1}{\varepsilon_0}\Big[\chi^{-1}\Delta\mathbf{p}\cdot\delta\mathbf{p}+\big(\chi_n^{-1}-\chi^{-1}\big)\Big(\Delta\mathbf{p}\cdot\overset{0}{\mathbf{n}}+\overset{0}{\mathbf{p}}\cdot\Delta\mathbf{n}\Big)\Big(\delta\mathbf{p}\cdot\overset{0}{\mathbf{n}}+\overset{0}{\mathbf{p}}\cdot\delta\mathbf{n}\Big)$$
$$+(\nabla\times\Delta\boldsymbol{\alpha}-\Delta\mathbf{p})\cdot(\nabla\times\delta\boldsymbol{\alpha}-\delta\mathbf{p})+\frac{1}{\xi_2}(\nabla\cdot\Delta\boldsymbol{\alpha})(\nabla\cdot\delta\boldsymbol{\alpha})\Big]\Big)dV=0. \tag{14}$$

From (14), the vanishing of the $\delta\mathbf{p}$ term gives $\Delta\mathbf{p}$ in terms of $\Delta\mathbf{n}$ and $\Delta\boldsymbol{\alpha}$, namely

$$\Delta\mathbf{p}=\frac{\chi}{1+\chi}(\nabla\times\Delta\boldsymbol{\alpha})+\frac{\chi_n-\chi}{(1+\chi)(1+\chi_n)}\Big[\overset{0}{\mathbf{n}}\cdot(\nabla\times\Delta\boldsymbol{\alpha})\Big]\overset{0}{\mathbf{n}}+\frac{\chi_n-\chi}{(1+\chi_n)\chi}\Big(\overset{0}{\mathbf{p}}\cdot\Delta\mathbf{n}\Big)\overset{0}{\mathbf{n}}. \tag{15}$$

By replacing the above equation in (14) and using the principal solution in (12), we obtain after some algebra

$$\big(\mathcal{P}^0_{,\mathbf{uu}}\Delta\mathbf{u}\big)\delta\mathbf{u}=\int_V\Big(k_1(\nabla\cdot\Delta\mathbf{n})(\nabla\cdot\delta\mathbf{n})+k_2\Big[\overset{0}{\mathbf{n}}(\nabla\times\Delta\mathbf{n})\Big]\Big[\overset{0}{\mathbf{n}}\cdot(\nabla\times\delta\mathbf{n})\Big]$$
$$+k_3\Big[\overset{0}{\mathbf{n}}\times(\tau\Delta\mathbf{n}+\nabla\times\Delta\mathbf{n})\Big]\cdot\Big[\overset{0}{\mathbf{n}}\times(\tau\delta\mathbf{n}+\nabla\times\delta\mathbf{n})\Big]$$
$$+\frac{1}{\varepsilon_0}\Big[\frac{1}{1+\chi}(\nabla\times\Delta\boldsymbol{\alpha})\cdot(\nabla\times\delta\boldsymbol{\alpha})+\frac{(\chi-\chi_n)(1+\chi)}{\chi^2(1+\chi_n)}\Big(\overset{0}{\mathbf{p}}\cdot\Delta\mathbf{n}\Big)\Big(\overset{0}{\mathbf{p}}\cdot\delta\overset{0}{\mathbf{n}}\Big)$$
$$+\frac{\chi-\chi_n}{(1+\chi)(1+\chi_n)}\Big[\overset{0}{\mathbf{n}}\cdot(\nabla\times\Delta\boldsymbol{\alpha})\Big]\Big[\overset{0}{\mathbf{n}}\cdot(\nabla\times\delta\boldsymbol{\alpha})\Big]$$
$$+\frac{\chi-\chi_n}{\chi(1+\chi_n)}\Big\{\Big[\overset{0}{\mathbf{n}}\cdot(\nabla\times\Delta\boldsymbol{\alpha})\Big]\Big(\overset{0}{\mathbf{p}}\cdot\delta\mathbf{n}\Big)+\Big(\overset{0}{\mathbf{p}}\cdot\Delta\mathbf{n}\Big)\Big[\overset{0}{\mathbf{n}}\cdot(\nabla\times\delta\boldsymbol{\alpha})\Big]\Big\}\Big]$$
$$+\frac{k}{\ell^2\xi_1}\Big(\overset{0}{\mathbf{n}}\cdot\Delta\mathbf{n}\Big)\Big(\overset{0}{\mathbf{n}}\cdot\delta\mathbf{n}\Big)+\frac{1}{\varepsilon_0\xi_2}(\nabla\cdot\Delta\boldsymbol{\alpha})(\nabla\cdot\delta\boldsymbol{\alpha})\Big)dV=0, \tag{16}$$

where we have defined, after eliminating $\mathbf{p}$, a new vector of unknowns $\mathbf{u}\equiv(\mathbf{n},\boldsymbol{\alpha})$.

The above equation can be recast, using Cartesian coordinates for all its field quantities, in the form

$$\big(\mathcal{P}^0_{,\mathbf{uu}}\Delta\mathbf{u}\big)\delta\mathbf{u}=\int_V\big[\mathcal{L}^{\nabla n\nabla n}_{ijkl}\Delta n_{i,j}\delta n_{k,l}+\mathcal{L}^{nn}_{ij}\Delta n_i\delta n_j$$
$$+\mathcal{L}^{\nabla nn}_{ijk}(\Delta n_{i,j}\delta n_k+\Delta n_k\delta n_{i,j})$$
$$+\mathcal{L}^{\nabla\alpha n}_{ijk}(\Delta\alpha_{i,j}\delta n_k+\Delta n_k\delta\alpha_{i,j})$$
$$+\mathcal{L}^{\nabla\alpha\nabla\alpha}_{ijkl}\Delta\alpha_{i,j}\delta a_{k,l}\big]dV=0, \tag{17}$$

where the coefficients in the above equation are defined by

$$\mathcal{L}^{\nabla n\nabla n}_{ijkl}\equiv k_1\delta_{ij}\delta_{kl}+(k_2-k_3)\overset{0}{n}_p\overset{0}{n}_q\varepsilon_{pij}\varepsilon_{qkl}+k_3(\delta_{ik}\delta_{jl}-\delta_{il}\delta_{jk}),$$
$$\mathcal{L}^{nn}_{ij}\equiv k_3\tau^2\delta_{ij}+\frac{k}{\ell^2\xi_1}\overset{0}{n}_i\overset{0}{n}_j+\frac{\varepsilon_0(e_0)^2(\chi-\chi_n)}{(1+\chi)(1+\chi_n)}\delta_{i3}\delta_{j3},$$
$$\mathcal{L}^{\nabla\alpha\nabla\alpha}_{ijkl}\equiv\frac{1}{\varepsilon_0(1+\chi)}\Big(\delta_{ik}\delta_{jl}-\delta_{il}\delta_{jk}+\frac{\chi-\chi_n}{1+\chi_n}\overset{0}{n}_p\overset{0}{n}_q\varepsilon_{pij}\varepsilon_{qkl}\Big)$$
$$+\frac{1}{\varepsilon_0\xi_2}\delta_{ij}\delta_{kl}, \tag{18}$$
$$\mathcal{L}^{\nabla nn}_{ijk}\equiv k_3\tau\Big(\overset{0}{n}_k\overset{0}{n}_q\varepsilon_{qij}-\varepsilon_{kij}\Big),$$
$$\mathcal{L}^{\nabla\alpha n}_{ijk}\equiv\frac{e_0(\chi_n-\chi)}{(1+\chi)(1+\chi_n)}\overset{0}{n}_r\varepsilon_{rij}\delta_{k3}.$$

We note here that most of the coefficients are not constant, i.e., they depend on x_3, through $\overset{0}{\mathbf{n}}(x_3)$ according to (12) if the twist is $\tau\neq0$.

Integration by parts of (17) yields in view of the arbitrariness of $\delta\mathbf{u}$ [$=(\delta\mathbf{n},\delta\boldsymbol{\alpha})$] the Euler-Lagrange equations for the twisted nematic device, as well as the natural boundary conditions. The governing equations for the system are, for $(x_1,x_2,x_3)\in\mathbb{R}^2\times[-\ell/2,\ell/2]$,

$$\mathcal{L}^{nn}_{ik}\Delta n_i-\big(\mathcal{L}^{\nabla n\nabla n}_{ijkl}\Delta n_{i,j}\big)_{,l}+\mathcal{L}^{\nabla nn}_{ijk}\Delta n_{i,j}-\big(\mathcal{L}^{\nabla nn}_{kli}\Delta n_i\big)_{,l}$$
$$+\mathcal{L}^{\nabla\alpha n}_{ijk}\Delta\alpha_{i,j}=0,$$
$$\big(\mathcal{L}^{\nabla\alpha\nabla\alpha}_{ijkl}\Delta\alpha_{i,j}\big)_{,l}+\big(\mathcal{L}^{\nabla\alpha n}_{kli}\Delta n_i\big)_{,l}=0. \tag{19}$$

Expanding the above equations gives a system of six governing equations for the six unknowns $\Delta\mathbf{u}$ (components of $\Delta\mathbf{n}$ and $\Delta\boldsymbol{\alpha}$); these equations form a homogeneous system of partial differential equations with nonconstant coefficients, which will be solved numerically for $\tau\neq0$.

The natural boundary conditions for $(x_1,x_2)\in\mathbb{R}^2$, $x_3=\pm\ell/2$ read (recall that the $\pm\mathbf{k}$ are the normals to the bounding surfaces of the TND)

$$\mathcal{L}^{\nabla\alpha\nabla\alpha}_{i3kl}\Delta\alpha_{k,l}+\mathcal{L}^{\nabla\alpha n}_{i3k}\Delta n_k=0. \tag{20}$$

An analytical solution of the above eigenvalue problem is not possible, save for the special case of $\tau=0$. A combined analytical and numerical technique will be introduced in the next section to solve the general case $\tau\neq0$.

D. Nondimensionalization

To simplify the numerical calculations and the presentation of results, we define the following dimensionless quantities

for the thickness (x_3), wave number [$\boldsymbol{\omega} \equiv (\omega_1,\omega_2)$], electric perturbation potential ($\boldsymbol{\alpha}$), and electric-field strength (ζ); for notational simplicity, henceforth we keep the same symbols for the thickness, electric perturbation potential, and wave numbers:

$$x_3/\ell \longrightarrow x_3, \quad \boldsymbol{\alpha}\sqrt{k\varepsilon_0} \longrightarrow \boldsymbol{\alpha}, \quad \boldsymbol{\omega}\ell \longrightarrow \boldsymbol{\omega}, \quad \zeta \equiv e_0\ell\sqrt{\frac{\varepsilon_0}{k}}, \tag{21}$$

and we parametrize the Frank-Oseen constants in (2),

$$k \equiv [(k_1)^2 + (k_2)^2 + (k_3)^2]^{1/2}, \quad r_i \equiv k_i/k, \tag{22}$$

leading to the following expressions for the coefficients introduced in (18):

$$\begin{aligned}
\mathcal{L}^{\nabla n\nabla n}_{ijkl} &= \frac{k}{\ell^2}\big[r_1\delta_{ij}\delta_{kl} + (r_2 - r_3)\overset{0}{n}_p\overset{0}{n}_q\varepsilon_{pij}\varepsilon_{pkl} \\
&\quad + r_3(\delta_{ik}\delta_{jl} - \delta_{il}\delta_{jk})\big], \\
\mathcal{L}^{nn}_{ij} &= \frac{k}{\ell^2}\left[r_3(\Delta\phi)^2\delta_{ij} + \frac{1}{\xi_1}\overset{0}{n}_i\overset{0}{n}_j + \frac{\zeta^2(\chi - \chi_n)\delta_{i3}\delta_{j3}}{(1+\chi)(1+\chi_n)}\right], \\
\mathcal{L}^{\nabla\alpha\nabla\alpha}_{ijkl} &= \frac{k}{\ell^2}\left[\frac{1}{1+\chi}\left(\delta_{ik}\delta_{jl} - \delta_{il}\delta_{jk} + \frac{\chi - \chi_n}{1+\chi_n}\overset{0}{n}_p\overset{0}{n}_q\varepsilon_{pij}\varepsilon_{qkl}\right)\right. \\
&\quad \left. + \frac{\delta_{ij}\delta_{kl}}{\xi_2}\right], \\
\mathcal{L}^{\nabla nn}_{ijk} &= \frac{k}{\ell^2}\left[r_3\Delta\phi\left(\overset{0}{n}_k\overset{0}{n}_q\varepsilon_{qij} - \varepsilon_{ijk}\right)\right], \\
\mathcal{L}^{\nabla\alpha n}_{ijk} &= \frac{k}{\ell^2}\left[\frac{\zeta(\chi_n - \chi)}{(1+\chi)(1+\chi_n)}\overset{0}{n}_r\varepsilon_{rij}\delta_{k3}\right],
\end{aligned} \tag{23}$$

where the quantities inside the brackets are dimensionless with leading terms of O(1). Use of these dimensionless quantities facilitates the numerical simulations. In particular, the choice of (22) is motivated by the need to provide an easy comparison of the anisotropic cases with the isotropic, one-constant approximation $k_1 = k_2 = k_3 = k$ (midpoint of the triangular domain used to plot the results). The optimal magnitude for the dimensionless penalty terms ξ_1 and ξ_2 is found to be in the order of 10^{-6}.

III. RESULTS

We begin this section by deriving an analytical solution for the three-dimensional nematic device in the absence of twist ($\tau = 0$), and we compare the results with the existing literature for this case. We then describe the finite-element method (FEM) used to solve the general case of arbitrary twist ($\tau \neq 0$) numerically, and we present the results obtained.

A. Nematic liquid crystal with zero twist

In the absence of twist in the nematic device ($\tau = 0$), this problem can be solved analytically in view of the constant coefficients of the governing differential equations in (19). A further simplification resulting from setting $\tau = 0$ in (12) and (18) is $\mathcal{L}^{\nabla nn}_{ijk} = 0$. By taking into account the constraints $\Delta n_1 = 0$ (resulting from the unit norm of the director) and $\Delta\alpha_{i,i} = 0$ (resulting from the Coulomb gauge), (19) simplifies into the following set of four PDEs for $(x_1,x_2,x_3) \in \mathbb{R}^2 \times [-1/2,1/2]$, in terms of the four independent variables Δn_2, Δn_3, $\Delta\alpha_2$, and $\Delta\alpha_3$:

$$\begin{aligned}
&r_1(\Delta n_{2,22} + \Delta n_{3,32}) + r_2(\Delta n_{2,33} - \Delta n_{3,23}) + r_3(\Delta n_{2,11}) = 0, \\
&r_1(\Delta n_{2,23} + \Delta n_{3,33}) + r_2(\Delta n_{3,22} - \Delta n_{2,32}) + r_3(\Delta n_{3,11}) \\
&\quad + (c_n - c)[\zeta(\Delta\alpha_{3,2} - \Delta\alpha_{2,3}) + \zeta^2\Delta n_3] = 0, \\
&(c - c_n)\zeta\,\Delta n_{3,3} + c(\Delta\alpha_{2,11} + \Delta\alpha_{2,22} + \Delta\alpha_{3,32}) \\
&\quad + c_n(\Delta\alpha_{2,33} - \Delta\alpha_{3,23}) = 0, \\
&(c_n - c)\zeta\,\Delta n_{3,2} + c(\Delta\alpha_{3,11} + \Delta\alpha_{2,23} + \Delta\alpha_{3,33}) \\
&\quad + c_n(\Delta\alpha_{3,22} - \Delta\alpha_{2,32}) = 0,
\end{aligned} \tag{24}$$

where the following new constants have been introduced for simplicity: $c \equiv 1/(1+\chi)$ and $c_n \equiv 1/(1+\chi_n)$.

The above homogeneous linear system is completed by the following boundary conditions for $(x_1,x_2) \in \mathbb{R}^2$, $x_3 = \pm 1/2$:

$$\begin{aligned}
&\Delta n_2 = 0,\ \Delta n_3 = 0; \quad \Delta\alpha_{2,23} + \Delta\alpha_{3,33} + \Delta\alpha_{3,11} = 0, \\
&\Delta\alpha_{2,3} - \Delta\alpha_{3,2} = 0.
\end{aligned} \tag{25}$$

The above first two relations (involving Δn_i) are essential boundary conditions due to the anchoring of the director at the two end plates, while the last two relations (involving $\Delta\alpha_i$) are the nontrivial natural boundary conditions (modified with the help of the Coulomb gauge to eliminate $\Delta\alpha_1$).

The bounded (in $\mathbb{R}^2 \times [-1/2,1/2]$) eigenmode $[\Delta n_2(x_i), \Delta n_3(x_i), \Delta\alpha_2(x_i), \Delta\alpha_3(x_i)]$ solution of the above linear system can be put in the form

$$\begin{aligned}
&[\Delta n_2, \Delta n_3, \Delta\alpha_2, \Delta\alpha_3] \\
&\quad = [i\,N_2(x_3), N_3(x_3), A_2(x_3), i\,A_3(x_3)]\exp[i(\omega_1 x_1 + \omega_2 x_2)].
\end{aligned} \tag{26}$$

Using the above representation in (24), one obtains the following four linear, homogeneous systems of ordinary differential equations for $\mathbf{V}(x_3) \equiv [N_2(x_3), N_3(x_3), A_2(x_3), A_3(x_3)]$, where $x_3 \in [-1/2,1/2]$:

$$\begin{aligned}
&r_1[(\omega_2)^2 N_2 + \omega_2 N_{3,3}] - r_2[N_{2,33} + \omega_2 N_{3,3}] \\
&\quad + r_3[(\omega_1)^2 N_2] = 0, \\
&r_1[\omega_2 N_{2,3} + N_{3,33}] - r_2[(\omega_2)^2 N_3 + \omega_2 N_{2,3}] - r_3[(\omega_1)^2 N_3] \\
&\quad + (c_n - c)[\zeta(\omega_2 A_3 - A_{2,3}) + \zeta^2\Delta N_3] = 0, \\
&(c - c_n)\zeta\,N_{3,3} + c\{-[(\omega_1)^2 + (\omega_2)^2]A_2 + \omega_2 A_{3,3}\} \\
&\quad + c_n[A_{2,33} - \omega_2 A_{3,3}] = 0, \\
&(c_n - c)\zeta\,\omega_2 N_3 + c[(\omega_1)^2 A_3 + \omega_2 A_{2,3} - A_{3,33}] \\
&\quad + c_n[(\omega_2)^2 A_3 - \omega_2 A_{2,3}] = 0,
\end{aligned} \tag{27}$$

plus the boundary conditions for $x_3 = \pm 1/2$:

$$\begin{aligned}
&N_2 = 0,\ N_3 = 0; \\
&\omega_2 A_{2,3} - A_{3,33} + (\omega_1)^2 A_3 = 0,\ A_{2,3} - \omega_2 A_3 = 0.
\end{aligned} \tag{28}$$

The above linear system (27) and its corresponding boundary conditions (28) admit a general solution of the form

$$\mathbf{V}(x_3) = \sum_{I=1}^{4}\left[\xi_I^S\mathbf{V}_S^I\sinh(\rho_I x_3) + \xi_I^C\mathbf{V}_C^I\cosh(\rho_I x_3)\right], \tag{29}$$

where ξ_I^S and ξ_I^C are the eigenmode amplitudes, to be subsequently determined with the help of the boundary conditions (28). The scalars ρ_I (roots of the system's characteristic equation) and the constants $\mathbf{V}_S^I \equiv [N_{2s}^I, N_{3c}^I, A_{2s}^I, A_{3c}^I]$ and $\mathbf{V}_C^I \equiv [N_{2c}^I, N_{3s}^I, A_{2c}^I, A_{3s}^I]$ satisfy

$$\mathbf{Q}(\omega_1,\omega_2,\rho_I)\cdot\mathbf{V}_S^I = \mathbf{Q}(\omega_1,\omega_2,\rho_I)\cdot\mathbf{V}_C^I = \mathbf{0}, \quad 1 \leqslant I \leqslant 4 \text{ (no sum in } I), \tag{30}$$

where the nonzero components of the 4×4 symmetric matrix $\mathbf{Q}(\omega_1,\omega_2,\rho)$ are given by

$$\begin{aligned}
Q_{11} &= r_1(\omega_2)^2 + r_3(\omega_1)^2 - r_2\rho^2,\\
Q_{12} &= \omega_2\rho(r_1 - r_2) = Q_{21},\\
Q_{13} &= 0 = Q_{31}, \quad Q_{14} = 0 = Q_{41},\\
Q_{22} &= r_1\rho^2 - r_3(\omega_1)^2 - r_2(\omega_2)^2 + (c - c_n)\zeta^2,\\
Q_{23} &= -(c - c_n)\rho\zeta = Q_{32},\\
Q_{24} &= (c - c_n)\rho\omega_2 = Q_{42},\\
Q_{33} &= c[(\omega_1)^2 + (\omega_2)^2] - c_n\rho^2,\\
Q_{34} &= -(c - c_n)\omega_2\rho = Q_{43},\\
Q_{44} &= c[\rho^2 - (\omega_1)^2] - c_n(\omega_2)^2.
\end{aligned} \tag{31}$$

A nontrivial solution for (30) is possible when

$$\det[\mathbf{Q}(\omega_1,\omega_2,\rho)] = 0. \tag{32}$$

The above equation is a fourth-order polynomial in ρ^2, which can be put in the form

$$\begin{aligned}
&(G(\rho)\{[\rho^2 - (\omega_2)^2]c_n - (\omega_1)^2 c\} + \zeta^2[\rho^2 - (\omega_1)^2 - (\omega_2)^2]c)\\
&\times[\rho^2 - (\omega_1)^2 - (\omega_2)^2] = 0,\\
&G(\rho) \equiv \Big\{ r_1\rho^2 - r_3(\omega_1)^2 - r_2(\omega_2)^2\\
&\qquad + \frac{[\rho\omega_2(r_1 - r_2)]^2}{r_2\rho^2 - r_3(\omega_1)^2 - r_1(\omega_2)^2}\Big\}(c - c_n)^{-1}.
\end{aligned} \tag{33}$$

Consequently, there are eight roots, $\pm\rho_I$, $1 \leqslant I \leqslant 4$, which are solutions of (32). The obvious root from (33), i.e., $(\rho_4)^2 = [(\omega_1)^2 + (\omega_2)^2]^{1/2}$, does not depend on ζ, and, as discussed subsequently, it corresponds to eigenmodes with no physical meaning. The remaining roots (which depend in general on ζ) can be either real or complex. Finding the dimensionless critical electric field ζ_c requires using the only information not yet taken into account, namely the boundary conditions (28). Introducing (29) into (28) will result in a homogeneous, linear system for the eight unknown amplitudes ξ_I^S, ξ_I^C; $1 \leqslant I \leqslant 4$; finding conditions for a nontrivial solution to this system (i.e., a solution in which at least one of the amplitudes is nonzero) will provide the sought-after critical electric field.

The 8×8 matrix resulting from using (29) in (28) can be rewritten in block form of two 4×4 matrices $\mathbf{M}^S$ and $\mathbf{M}^C$, corresponding to ξ_I^S and ξ_I^C, respectively, thus giving (after considerable algebraic manipulations) the sought-after condition for the critical electric field by

$$\det[\mathbf{M}^S(\omega_1,\omega_2,\zeta)] = 0, \quad \det[\mathbf{M}^C(\omega_1,\omega_2,\zeta)] = 0; \tag{34}$$

$$\begin{aligned}
M_{1J}^S &= \frac{(\rho_J)^2 - (\omega_1)^2 - (\omega_2)^2}{[r_2(\rho_J)^2 - r_1(\omega_2)^2 - r_3(\omega_1)^2]G(\rho_J)}\tanh(\rho_J\ell/2),\\
M_{1J}^C &= \frac{(\rho_J)^2 - (\omega_1)^2 - (\omega_2)^2}{[r_2(\rho_J)^2 - r_1(\omega_2)^2 - r_3(\omega_1)^2]G(\rho_J)}\coth(\rho_J\ell/2),\\
M_{2J}^S &= \frac{(\rho_J)^2 - (\omega_1)^2 - (\omega_2)^2}{\rho_J G(\rho_J)} = M_{2J}^C \equiv M_{2J},\\
M_{3J}^S &= \frac{(\omega_1)^2}{\rho_J} = M_{3J}^C \equiv M_{3J},\\
M_{4J}^S &= \frac{(\rho_J)^2 - (\omega_2)^2}{\rho_J} = M_{4J}^C \equiv M_{4J},
\end{aligned}$$

where the quantity $G(\rho)$ is defined in (33).

A word of caution here: as one can see from (33), one of its roots, $(\rho_4)^2 = (\omega_1)^2 + (\omega_2)^2$, is independent of ζ, and the corresponding eigenmodes with amplitudes ξ_4^S and ξ_4^C are physically meaningless for they have zero components of the director and the electric displacement. Setting $\xi_4^S = \xi_4^C = 0$, one must satisfy two sets of four boundary conditions with two sets of three amplitudes. Fortunately, one can show from (33) and the definitions of the coefficients M_{IJ} in (34) that

$$c\zeta^2 M_{2J} - cM_{3J} + c_n M_{4J} = 0, \quad 1 \leqslant J \leqslant 3, \tag{35}$$

in which case (34) reduces to finding the determinants of two 3×3 matrices:

$$\begin{aligned}
&\det\left[M_{IJ}^S(\omega_1,\omega_2,\zeta)\right] = 0,\\
&\det\left[M_{IJ}^C(\omega_1,\omega_2,\zeta)\right] = 0; \quad 1 \leqslant I, \quad J \leqslant 3.
\end{aligned} \tag{36}$$

The lowest $\zeta > 0$ roots of the above two equations (36) are denoted by $\zeta_m^S(\omega_1,\omega_2)$ and $\zeta_m^C(\omega_1,\omega_2)$, respectively, and hence the dimensionless critical electric field ζ_c is

$$\zeta_c = \min_{(\omega_1,\omega_2)\in\mathbb{R}^2}\left[\zeta_m^S(\omega_1,\omega_2), \zeta_m^C(\omega_1,\omega_2)\right], \tag{37}$$

where only the positive quadrant of $\mathbb{R}^2$ needs to be investigated, since the squares of the wave numbers appear in the governing equations.

Further simplification of this result is possible, by assuming $r_3 = 0$ or equivalently $\omega_1 = 0$, since only the product of these constants appears in the components of $\mathbf{Q}(\omega_1,\omega_2,\rho)$ in (31). This simplification is relevant since our calculations for $r_3 > 0$ show that the minimum dimensionless electric field, found using (37), always corresponds to $\omega_1 = 0$ (a result in agreement with [21] for the 2D case). For this case, one can see that (33) has another root that is independent of ζ, namely $(\rho_3)^2 = (\omega_2)^2$. The physically meaningful eigenmodes are now the ones corresponding to the remaining two roots $(\rho_1)^2$ and $(\rho_2)^2$ of (33), which satisfy

$$c_n r_1 r_2[\rho^2 - (\omega_2)^2]^2 + c(c - c_n)\zeta^2[r_2\rho^2 - r_1(\omega_2)^2] = 0. \tag{38}$$

Consequently from (34) and (36) one obtains the following equations for the dimensionless lowest electric fields $\zeta_m^S(0,\omega_2)$

and $\zeta_m^C(0,\omega_2)$, respectively:

$$\frac{\rho_1 \tanh(\rho_1/2)}{r_2(\rho_1)^2 - r_1(\omega_2)^2} - \frac{\rho_2 \tanh(\rho_2/2)}{r_2(\rho_2)^2 - r_1(\omega_2)^2} = 0,$$
$$\frac{\rho_1 \coth(\rho_1/2)}{r_2(\rho_1)^2 - r_1(\omega_2)^2} - \frac{\rho_2 \coth(\rho_2/2)}{r_2(\rho_2)^2 - r_1(\omega_2)^2} = 0. \tag{39}$$

By investigating the lowest ζ roots of the above two transcendental equations [since ρ_1 and ρ_2 are functions of ζ found from (38)], it can be shown that for adequately low values of r_2/r_1, the critical wave number corresponds to $\zeta_c = \zeta_m^S(0,\omega_{2c})$, where $\omega_{2c} > 0$, thus indicating a finite-wavelength critical mode, termed *periodic Freedericksz transitions*, as found by [16] and discussed in detail in [17].

The analytical results for $\zeta_m^S(\omega_1,\omega_2)$ and $\zeta_m^C(\omega_1,\omega_2)$ are used to check the FEM calculations reported below.

B. Finite-element algorithm

The numerical solution technique for the eigenvalue problem (19) and (20) [plus of course the essential boundary condition (10)] for the general case $\tau \neq 0$ is based on the Fourier transform of $\Delta\mathbf{u}$ in the x_1,x_2 directions ($\mathbb{R}^2$) and a finite-element discretization along x_3.

Denoting the Fourier transform of quantities $\Delta\boldsymbol{\alpha}(x_1,x_2,x_3)$ and $\Delta\mathbf{n}(x_1,x_2,x_3)$ by $\Delta\mathbf{A}(\omega_1,\omega_2,x_3)$ and $\Delta\mathbf{N}(\omega_1,\omega_2,x_3)$ and using the Fourier-Plancherel identity, (17) yields

$$\begin{aligned}(\mathcal{P}^0_{,\mathbf{uu}}\Delta\overline{\mathbf{u}})\delta\mathbf{u} = \int_{\mathbb{R}^2}\Bigg[\int_{-1/2}^{+1/2} &\big(\mathcal{L}^{\nabla n\nabla n}_{i3k3}\Delta\overline{N}_{i,3}\delta N_{k,3} - i\omega_a\mathcal{L}^{\nabla n\nabla n}_{iak3}\Delta\overline{N}_i\delta N_{k,3} + i\omega_\beta\mathcal{L}^{\nabla n\nabla n}_{i3k\beta}\Delta\overline{N}_{i,3}\delta N_k + \omega_a\omega_\beta\mathcal{L}^{\nabla n\nabla n}_{iak\beta}\Delta\overline{N}_a\delta N_\beta\\
&+\mathcal{L}^{\nabla nn}_{i3k}(\Delta\overline{N}_{i,3}\delta N_k + \Delta\overline{N}_k\delta N_{i,3}) + i\omega_\alpha\mathcal{L}^{\nabla nn}_{iak}(\Delta\overline{N}_k\delta N_i - \Delta\overline{N}_i\delta N_k) + \mathcal{L}^{nn}_{ij}\Delta\overline{N}_i\delta N_j\\
&+\mathcal{L}^{\nabla a\nabla a}_{i3k3}\Delta\overline{A}_{i,3}\delta A_{k,3} - i\omega_a\mathcal{L}^{\nabla a\nabla a}_{iak3}\Delta\overline{A}_i\delta A_{k,3} + i\omega_\beta\mathcal{L}^{\nabla a\nabla a}_{i3k\beta}\Delta\overline{A}_{i,3}\delta A_k + \omega_a\omega_\beta\mathcal{L}^{\nabla a\nabla a}_{iak\beta}\Delta\overline{A}_i\delta A_k\\
&+\mathcal{L}^{\nabla an}_{i3k}(\Delta\overline{A}_{i,3}\delta N_k + \Delta\overline{N}_k\delta A_{i,3}) + i\omega_a\mathcal{L}^{\nabla an}_{iak}(\Delta\overline{N}_k\delta A_i - \Delta\overline{A}_i\delta N_k)\big)dx_3\Bigg]d\omega_1 d\omega_2 = 0,\end{aligned} \tag{40}$$

where a bar ($\overline{f}$) denotes complex conjugation of the quantity involved (f).

A sufficient condition for loss of positive definiteness of the functional in (40) is the loss of positive definiteness of its integrand in $[-1/2,1/2]$, which corresponds to eigenmodes of the type $\Delta\mathbf{u} = \Delta\mathbf{U}\exp[i(\omega_1 x_1 + \omega_2 x_2)]$. A finite-element discretization of $\Delta\mathbf{A},\Delta\mathbf{N}$ in the interval $[-1/2,1/2]$ is used to check the loss of positive definiteness of this functional $\forall(\omega_1,\omega_2) \in \mathbb{R}^2$, thus finding the lowest (critical) electric field e_0^c at the onset of a Freedericksz bifurcation. For each pair $(\omega_1,\omega_2) \in \mathbb{R}^2$, the interval $[-1/2,1/2]$ is divided in N equal segments (i.e., finite elements). A linear interpolation function is then used for each resulting two-node element where each node I has six degrees of freedom defined via the column vector $\Delta\mathbf{U}^I \equiv [\Delta N_1^I,\Delta N_2^I,\Delta N_3^I,\Delta A_1^I,\Delta A_2^I,\Delta A_3^I]$. The resulting functional in (40) can then be put in matrix form:

$$(\mathcal{P}_{,\mathbf{uu}}\Delta\overline{\mathbf{u}})\delta\mathbf{u} = [\Delta\overline{\mathbf{U}}]^T \cdot \mathbf{K}(\omega_1,\omega_2,\zeta) \cdot [\Delta\mathbf{U}], \tag{41}$$

where $[\Delta\mathbf{U}] = [\Delta\mathbf{U}^1,\Delta\mathbf{U}^2,\ldots,\Delta\mathbf{U}^{N+1}]$ is the global $6(N+1)$ column vector of the nodal degree of freedom, and $\mathbf{K}$ is the corresponding $[6(N+1)] \times [6(N+1)]$ stiffness matrix, also termed the *stability matrix*, which is Hermitian and therefore has real eigenvalues.

In the absence of an electric field ($\zeta = 0$), the stability matrix $\mathbf{K}(\omega_1,\omega_2,0)$ is always positive definite. The sought-after critical value of the electric field ζ_c is the lowest $\zeta > 0$ root of $\det\mathbf{K}(\omega_1,\omega_2,\zeta) = 0$ over all $(\omega_1,\omega_2) \in \mathbb{R}^2$, namely

$$\det\mathbf{K}(\omega_1,\omega_2,\zeta_m) = 0, \quad \zeta_c = \min_{(\omega_1,\omega_2)\in\mathbb{R}^2}\zeta_m(\omega_1,\omega_2). \tag{42}$$

For a given (ω_1,ω_2) we find ζ_m, the lowest root of $\det\mathbf{K} = 0$, by a straightforward procedure where ζ is increased away from zero by $\Delta\zeta = 10^{-1}$ followed by an examination of the sign of the minimum eigenvalue of $\mathbf{K}$ and then using a bisection method to increase the accuracy of ζ_m. In this way, ζ_m is evaluated in a dense grid in the Fourier space domain $(\omega_1,\omega_2) \in [-10,10] \times [-10,10]$ using increments of $\Delta\omega_i = 10^{-3}$. Due to symmetry $\mathbf{K}(\omega_1,\omega_2,\zeta) = \overline{\mathbf{K}}(-\omega_1,-\omega_2,\zeta)$ and thus only half of the above interval is scanned; hence in all calculations we evaluate ζ_m in the domain $(\omega_1,\omega_2) \in [-10,10] \times [0,10]$. Although symmetry considerations can further reduce the scanned domain to half, for uniformity and to better depict the location of the critical eigenmode, in Fig. 2 we plot results in the domain $(\omega_1,\omega_2) \in [-10,10] \times [0,10]$.

In the calculations reported here, we use dimensionless penalty parameters $\xi_1 = \xi_2 = 10^{-6}$ in order to impose the unit length of the director vector $\mathbf{n}$ and the Coulomb gauge condition, as discussed in the potential energy definition (9). To avoid locking (and hence an overly stiff system), a standard reduced integration scheme with one Gauss point per element is used to integrate the Coulomb gauge part and the unit length director constraint in the x_3 integral appearing in (40). For the remaining terms in that integral, the integration is carried out using two Gauss points per element.

The mesh size (all calculations used a mesh of $N = 40$ equal length elements) as well as the value of penalty parameters and the adopted integration scheme are selected by comparing the numerically calculated $\zeta_m(\omega_1,\omega_2)$ to its analytical counterpart for $\tau = 0$ given by Eq. (36) with the relative error required to be within less than 0.1%.

C. Results for the twisted nematic device

We start by presenting in Fig. 2 the $\zeta_m(\omega_1,\omega_2)$ contours for the 5CB twisted nematic device ($k_1 = 6.2pN$, $k_2 = 3.9pN$, $k_3 = 8.2pN$, $\chi_n = 17.5$, and $\chi = 6$) for four different values of the twist angle $\Delta\phi = 0$, $\pi/2$, π, and $3\pi/2$, with the

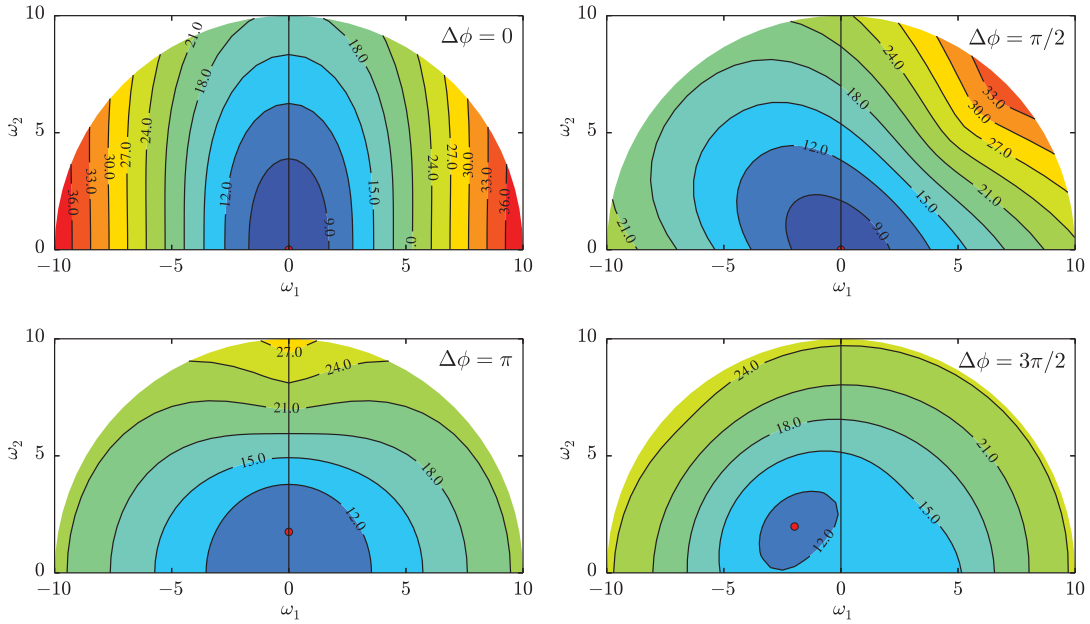

FIG. 2. Contours of the lowest dimensionless electric field ζ_m at the onset of bifurcation, as a function of the dimensionless eigenmode wave numbers ω_1 and ω_2, for four different values of the twist angle $\Delta\phi$ calculated for a 5CB liquid crystal. Its lowest (critical) value ζ_c occurs at the location indicated by a small (red) dot; notice that for $\Delta\phi = 0,\pi/2$, the critical electric field corresponds to a long-wavelength eigenmode $(\omega_{1c},\omega_{2c}) = (0,0)$, while for $\Delta\phi = \pi,3\pi/2$, the minimum corresponds to a finite-wavelength eigenmode.

last value typical of a STND (see [4]). The lowest (critical) value of the dimensionless electric field ζ_c occurs at the location indicated by a small (red) dot; notice that for the two lower values of the twist angle $\Delta\phi = 0,\ \pi/2$, the critical electric field corresponds to a long-wavelength eigenmode $(\omega_{1c},\omega_{2c}) = (0,0)$, in which case a simple 1D analysis (where all field quantities depend solely on the thickness coordinate) can give ζ_c. For the two larger twist angles $\Delta\phi = \pi,\ 3\pi/2$, the minimum corresponds to a finite-wavelength eigenmode, and hence a 3D analysis is necessary. Notice the additional symmetry in the graphs of Fig. 2. For the case of twist angles $\Delta\phi = 0,\ \pi$, there is a symmetry of ζ_m with respect to the coordinate axes, since ζ_m is independent of the wave-number sign. Indeed, as seen in the analysis for $\tau = 0$, the governing equations depend on the square of each wave number and hence $\zeta_m(\omega_1,\omega_2) = \zeta_m(-\omega_1,\omega_2) = \zeta_m(\omega_1,-\omega_2)$. For the case of twist angles $\Delta\phi = \pi/2,\ 3\pi/2$, there is a symmetry of ζ_m with respect to the diagonals, since a rotation of the axes

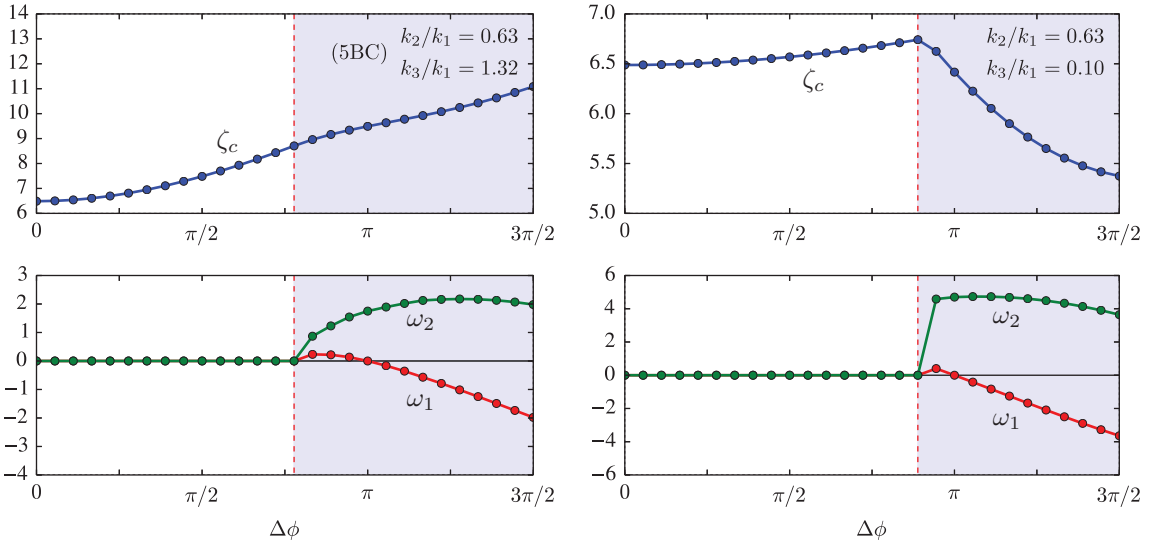

FIG. 3. Dependence of the dimensionless critical electric field ζ_c (top) and the corresponding dimensionless eigenmode wave numbers ω_1 and ω_2 (bottom) on the twist angle $\Delta\phi$ for two different sets of Frank-Oseen constants. Notice that above a certain value of $\Delta\phi$, the critical eigenmode changes from global to local (from infinite to finite wavelengths), as indicated by a dashed (red) vertical line. The electric susceptibility constants ($\chi_n = 17.5$ and $\chi = 6.0$) are the same in both cases. Observe the critical electric field $\zeta_c(\Delta\phi)$ in the liquid crystal with the lower bend constant $k_3/k_1 = 0.1$ (right) that drops below its lowest value in the global mode regime, e.g., $\zeta_c(3\pi/2) < \zeta_c(0)$.

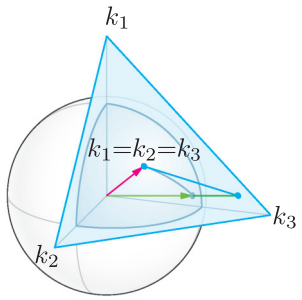

FIG. 4. Gnomonic projection used in plotting the influence of the three Frank-Oseen constants k_i on the critical eigenmode and corresponding electric field; the projection is motivated by the need to provide an easy comparison of the anisotropic cases with the isotropic, one-constant approximation $k_1 = k_2 = k_3 = k$ (midpoint of the triangular domain).

by $\pm\pi/2$ leaves the problem unchanged and $\zeta_m(\omega_1,\omega_2) = \zeta_m(\omega_2,\omega_1)$. For twist angles that are not integral multiples of $\pi/2$, no such symmetry exists and hence we need to scan the entire domain, $(\omega_1,\omega_2) \in [-10,10] \times [0,10]$.

The dependence of the dimensionless critical electric field ζ_c (top) and the corresponding dimensionless eigenmode wave numbers ω_1, ω_2 (bottom) on the twist angle $\Delta\phi$ is presented in Fig. 3 for two different sets of Frank-Oseen constants: $k_2/k_1 = 0.63, k_3/k_1 = 1.32$ (5CB values, left) and $k_2/k_1 = 0.63, k_3/k_1 = 0.10$ (right). In all calculations, the electric susceptibility constants are the same ($\chi_n = 17.5, \chi = 6.0$) and correspond to 5CB. Notice that above a certain value of $\Delta\phi$, the critical eigenmode changes from global to local (from infinite to finite wavelengths) for both cases. For the 5CB liquid crystal, the critical electric field ζ_c is a monotonically increasing function of the twist angle $\Delta\phi$; hence the lowest critical electric field for that liquid crystal occurs for $\Delta\phi = 0$. In contrast, the liquid crystal with the lower bend constant $k_3/k_1 = 0.1$ (right), after an initial increase of $\zeta_c(\Delta\phi)$ in the region where the critical mode is global, shows a significant drop in $\zeta_c(\Delta\phi)$ in the region where the critical mode is local; this decrease is so important that for adequately high twist angles, the critical electric field drops below its lowest value in the global mode regime, e.g., $\zeta_c(3\pi/2) < \zeta_c(0)$.

The influence of the dimensionless Frank-Oseen constants k_1, k_2, and k_3 on the critical eigenmode and corresponding dimensionless critical electric field are presented, respectively, in Figs. 5 and 6. In all these calculations, the electric susceptibility constants are $\chi_n = 17.5, \chi = 6.0$ and correspond to 5CB. The results are plotted using the *gnomonic projection* as depicted in Fig. 4; one-eighth of the surface of the sphere is thus mapped on an equilateral triangle. This projection displays all great circles as straight lines by casting surface points of the sphere onto a tangent plane, each landing where a ray from the center of the sphere passes through the point on the surface and then onto the plane.

More specifically, Fig. 5 records the contours of $\Omega_c \equiv [(\omega_{1c})^2 + (\omega_{2c})^2]^{1/2}$, corresponding to the critical dimensionless electric field ζ_c, as functions of the dimensionless Frank-Oseen constants k_i, for four different values of the twist angle $\Delta\phi$. The noncolored (white) area in the above graphs corresponds to global (long-wavelength) critical eigenmodes

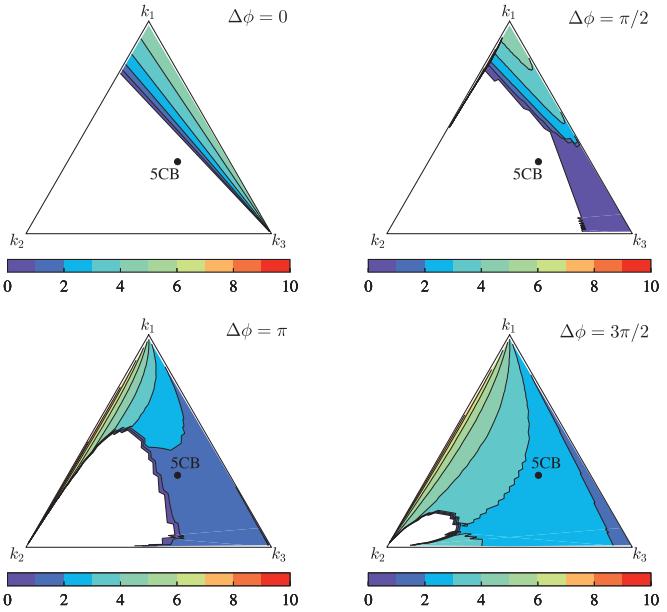

FIG. 5. Influence of the dimensionless Frank-Oseen constants k_1, k_2, and k_3 on the critical eigenmode. Contours of $\Omega_c \equiv [(\omega_{1c})^2 + (\omega_{2c})^2]^{1/2}$, corresponding to the critical dimensionless electric field ζ_c, are presented in gnomonic projection (see the inset) as functions of k_i for four different values of the twist angle $\Delta\phi$. The noncolored (white) area in the above graphs corresponds to global (long-wavelength) critical eigenmodes $\Omega_c = 0$. Results for the Frank-Oseen constants of the 5CB liquid crystal are indicated by a small (black) dot.

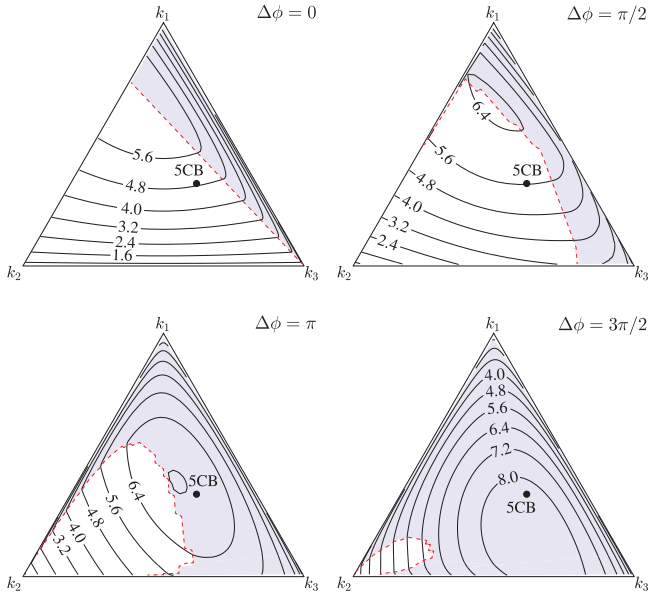

FIG. 6. Influence of the dimensionless Frank-Oseen constants k_1, k_2, and k_3 on the critical electric field. Contours of the critical dimensionless electric field ζ_c are presented in gnomonic projection (see the inset) as functions of k_i for four different values of the twist angle $\Delta\phi$. The unshaded (white) area in the above graphs corresponds to global (long-wavelength) critical eigenmodes $\Omega_c = 0$, while the shaded (gray) area corresponds to local (finite-wavelength) critical eigenmodes $\Omega_c > 0$, with the boundary of the two regions depicted by a dashed (red) line. Results for the Frank-Oseen constants of the 5CB liquid crystal are indicated by a small (black) dot.

$\Omega_c = 0$. Results for the 5CB liquid crystal are indicated by a small (black) dot.

The analytical results for the zero twist device ($\tau = 0$) presented in Sec. III A give a critical eigenmode with $\omega_{1c} = 0$ for all values of the Frank-Oseen constants, including the case $k_3 > 0$. This result is independently verified by the FEM calculations. Consequently, since ω_1 and r_3 ($\equiv k_3/k$) appear together as a product in (31), Fig. 5(a) shows, as expected, $\Omega_c = \omega_{2c}$ independent of the bend constant k_3. For adequately low values of the twist constant k_2, the critical eigenmode corresponds to a finite wave number $\Omega_c = \omega_{2c} > 0$ (periodic Freedericksz transition found by the authors of [16] and discussed in detail in [17]), which is a solution of (39). For this case, the solution of (39) agrees with the FEM numerical result.

Notice, by comparing the four different graphs in Fig. 5, that the increase of twist angle $\Delta\phi$ reduces the domain in parameter space corresponding to a global critical eigenmode ($\Omega_c = 0$). Calculations for the highest value of $\Delta\phi = 3\pi/2$ (typical of STND) show a local critical eigenmode $\Omega_c > 0$ for most of the parameter space investigated in Fig. 5(d). One should also mention at this point the possibility of abrupt changes in the critical wave numbers for small variations of Frank-Oseen constants, as seen most prominently in Fig. 5(b) for low values of k_3/k.

The influence of the dimensionless Frank-Oseen constants k_1, k_2, and k_3 on the critical electric field is presented in Fig. 6. Contours of the critical dimensionless electric field, ζ_c, are presented as functions of k_i for four different values of the twist angle $\Delta\phi$. The unshaded (white) area in the above graphs corresponds to global (long-wavelength) critical eigenmodes $\Omega_c = 0$, while the shaded (gray) area corresponds to local (finite-wavelength) critical eigenmodes $\Omega_c > 0$ with the boundary of the two regions depicted by a dashed (red) line. Results for the 5CB liquid crystal are indicated by a small (black) dot.

The results in Fig. 6 show that for a given angle of twist $\Delta\phi$, the dimensionless critical electric field ζ_c increases with increasing k_2 and k_3, although far from monotonically, as an observation of Figs. 6(b) and 6(c) can show. For all angles of twist, the lowest critical load occurs at the corner corresponding to the lowest values of k_2 and k_3.

Having explored the influence of the Frank-Oseen parameters on the stability of the TND, our attention now turns to the dependence of the critical electric field and the corresponding eigenmode on the electric susceptibility constants χ and χ_n in directions parallel and perpendicular to the director $\mathbf{n}$, respectively, with the results plotted in Fig. 7. Contours of ζ_c as functions of χ and $\Delta\chi \equiv \chi_n - \chi$ [since the governing equation depends on this difference, as seen from (18)] are plotted for three different values of $\Delta\phi$. The unshaded (white) area in the above graphs corresponds to global (long-wavelength) critical eigenmodes $\Omega_c = 0$, while the shaded (gray) area corresponds to local (finite-wavelength) critical eigenmodes $\Omega_c > 0$ with the boundary of the two regions depicted by a dashed (red) line. In all calculations, the Frank-Oseen constants are those of the 5CB liquid crystal, while the small (black) dots indicate results where the electric susceptibilities also correspond to 5CB.

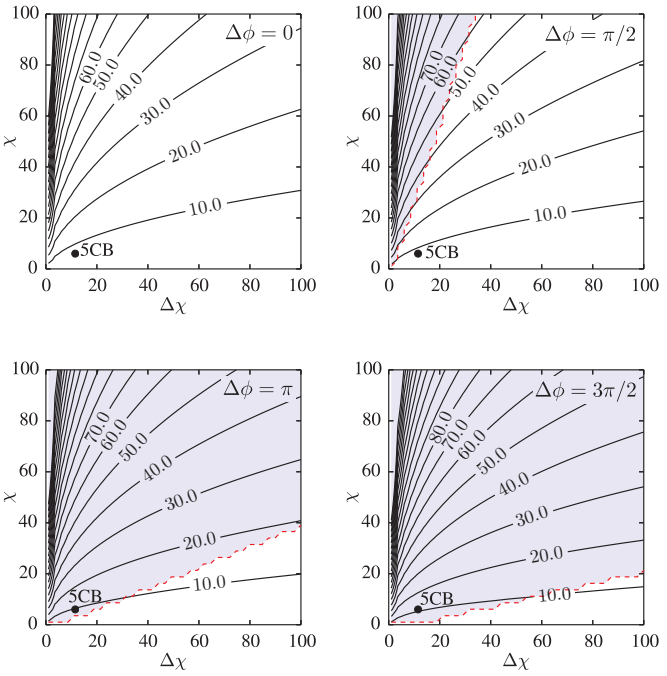

FIG. 7. Influence of electric susceptibility constants χ and χ_n on the critical electric field. Contours of ζ_c are presented as functions of χ and $\Delta\chi \equiv \chi_n - \chi$ for different values of $\Delta\phi$. The unshaded (white) area in the above graphs corresponds to global (long-wavelength) critical eigenmodes $\Omega_c = 0$, while the shaded (gray) area corresponds to local (finite-wavelength) critical eigenmodes $\Omega_c > 0$ with the boundary of the two regions depicted by a dashed (red) line. In all calculations, the Frank-Oseen constants are those of the 5CB liquid crystal, while the small (black) dots indicate results where the susceptibilities are also those of the 5CB.

The plots in Fig. 7 show that for fixed Frank-Oseen constants, the critical electric field increases monotonically with both χ and $\Delta\chi$, but it is considerably more sensitive to increases of χ than to increases of $\Delta\chi$, particularly for the lower values of χ. Moreover, these results show that the dependence of the critical electric field on the electric susceptibility is almost insensitive to the angle of twist $\Delta\phi$, as one can observe by comparing the four different graphs in Fig. 7, in contrast to the corresponding results on the Frank-Oseen constants. Nevertheless, the trend of increasing ζ_c with increasing $\Delta\phi$, for the same set of material parameters, persists, as one can see by comparing the three different graphs of Fig. 7. Also, increasing the twist angle results in increasing the domain in susceptibility space where the critical eigenmode is local, a trend already observed in Fig. 5.

The calculations in Fig. 3 show that for certain values of the Frank-Oseen constants, the critical electric field can decrease with the angle of twist to the point that for substantially large angles it can fall below its value for zero twist [usually a local minimum in the $\zeta_c(\Delta\phi)$]. To get a better idea of this phenomenon, we are depicting in Fig. 8 the contours of constant $\zeta_c(3\pi/2) - \zeta_c(0)$ as functions of k_i. Again, in these calculations the electric susceptibility constants are $\chi_n = 17.5, \chi = 6.0$, and they correspond to 5CB. The range

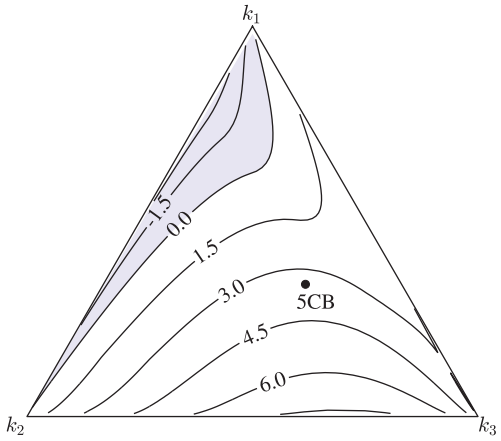

FIG. 8. Influence of the dimensionless Frank-Oseen constants k_1, k_2, and k_3 on the dropping of the critical electric field for the supertwisted nematic device (STND) presented in gnomonic projection. Contours of the difference of critical dimensionless electric field $\zeta_c(3\pi/2) - \zeta_c(0)$ as functions of the ratios k_2/k_1 and k_3/k_1. Results for the 5CB liquid crystal are indicated by a small (black) dot.

of the Frank-Oseen parameters where $\zeta_c(3\pi/2) - \zeta_c(0) < 0$ is indicated by gray shading.

Results in Fig. 8 show that lowering the bend constant in liquid crystals is more effective than lowering their twist counterpart (assuming a fixed splay constant) if one wants to achieve a low critical electric field by producing a STDN out of the liquid crystal at hand. The price to pay in achieving this critical electric field reduction by using a large twist angle $\Delta\phi = 3\pi/2$ is the most likely change of the critical mode from global to local, as seen in Figs. 5(d) and 6(d).

The systematic investigation, based on 3D analysis, presented above for the influence of the Frank-Oseen and electric susceptibility constants of TNDs on the critical (lowest) electric field and corresponding eigenmode gives the range of these parameters where the onset of bifurcation in these devices (Freedericksz transition) is global or local in nature and calculates the associated wavelengths for the latter case. These findings could be useful in guiding liquid-crystal selection for applications, since lowering the critical electric field reduces the energy consumption of the device, but the presence of a short-wavelength mode might need to be taken into account in the design.

IV. CONCLUSION

The object of this investigation is a fully three-dimensional analysis of the Freedericksz transition phenomenon in twisted nematic devices (TNDs) from the standpoint of bifurcation theory, using the recently proposed [21] coupled electromechanical variational formulation.

More specifically, we investigate the stability of the principal solution of the TND, consisting of a finite liquid-crystal layer strongly anchored between two infinite parallel plates and subjected to a transverse (i.e., normal to the plates) electric field. By scanning a wide range of the liquid crystal's material parameter space, we establish whether the lowest electric field corresponds to a global mode, with an eigenmode depending solely on the layer thickness coordinate (and thus captured by a 1D analysis), or to a local one (termed the periodic Freedericksz transition), with an eigenmode that has finite wavelengths in one or both directions parallel to the plate (and thus requiring a full 3D modeling). In contrast to existing analysis of TNDs that use perturbation methods involving 1D or 2D approximations for the director field, the present 3D model considers all possible bounded eigenmodes in order to select the critical electric field.

For arbitrary values of the TND twist angle, no analytical solution can be found, and a mixed analytical and numerical technique, combining finite-element discretization for the thickness coordinate with a Fourier transform for the remaining coordinates, is used to solve the bifurcation problem at hand. For the special case of zero twist, an analytical solution is possible; this solution is used to compare our results with the existing literature on periodic Freedericksz transitions and as a highly nontrivial check for the numerical algorithm developed for the general case.

Our calculations show that a device with a global critical mode for low values of twist invariably shows a local critical mode once the twist angle exceeds a certain level, depending on the constitutive parameters of the liquid crystal. Also, a monotonically increasing critical electric field as a function of the twist angle is not always the case, as our calculations have shown for liquid crystals with a low-twist Frank-Oseen constant.

The systematic investigation, based on 3D analysis, presented above for the influence of the Frank-Oseen and electric susceptibility constants of TNDs on the critical (lowest) electric field and corresponding eigenmode gives the range of these parameters where the onset of bifurcation in these devices (the Freedericksz transition) is global or local in nature and calculates the associated wavelengths for the latter case. These results could be useful in guiding liquid-crystal selection for applications, since lowering the critical electric field reduces the energy consumption of the device, but the presence of a short-wavelength mode might need to be taken into account in the design. Moreover, the continuum mechanics-based methodology introduced here is applicable to a wider class of problems involving the stability of devices involving liquid crystals (methodology that can be generalized to include nematic elastomers; see [21]), problems that, in addition to their theoretical interest, are at the heart of exciting new technological developments.

ACKNOWLEDGMENTS

The work of G.I.S. has been funded by a postdoctoral fellowship from the École Polytechnique. The authors would like to thank an anonymous reviewer for pointing out the work of [16] and the more recent one by [20] and for making helpful suggestions to improve our paper. K.D. would like to acknowledge partial support from CNRS (PEPS-INSIS programme) as well as from the European Research Council (ERC) under the European Union's Horizon 2020 research and innovation program (Grant Agreement No. 636903).

[1] V. Freedericksz and A. Repiewa, Z. Phys. **42**, 532 (1927).
[2] V. Freedericksz and V. Zolina, Trans. Faraday Soc. **29**, 919 (1933).
[3] M. Schadt and W. Helfrich, Appl. Phys. Lett. **18**, 127 (1971).
[4] T. J. Scheffer and J. Nehring, Appl. Phys. Lett. **45**, 1021 (1984).
[5] H. L. Ong, J. Appl. Phys. **64**, 614 (1988).
[6] C. Oseen, Trans. Faraday Soc. **29**, 883 (1933).
[7] H. Zocher, Trans. Faraday Soc. **29**, 945 (1933).
[8] F. C. Frank, Discuss. Faraday Soc. **25**, 19 (1958).
[9] J. L. Ericksen, Arch. Ration. Mech. Anal. **10**, 189 (1962).
[10] F. Leslie, Arch. Ration. Mech. Anal. **28**, 265 (1968).
[11] J. L. Ericksen, J. Elast. **87**, 95 (2007).
[12] P. de Gennes and J. Prost, *The Physics of Liquid Crystals* (Clarendon, Oxford, 1993).
[13] I. Stewart, *The Static and Dynamic Continuum Theory of Liquid Crystals: A Mathematical Introduction*, Liquid Crystals Book Series (Taylor & Francis, London, 2004).
[14] R. H. Self, C. P. Please, and T. J. Sluckin, Eur. J. Appl. Math. **13**, 1 (2002).
[15] P. Biscari and P. Cesana, Contin. Mech. Thermodyn. **19**, 285 (2007).
[16] F. Lonberg and R. B. Meyer, Phys. Rev. Lett. **55**, 718 (1985).
[17] E. Virga, *Variational Theories for Liquid Crystals*, Applied Mathematics and Mathematical Computation (Chapman & Hall, London, 1994).
[18] K. H. Yang, Appl. Phys. Lett. **43**, 171 (1983).
[19] R. Hirning, W. Funk, H. Trebin, M. Schmidt, and H. Schmiedel, J. Appl. Phys. **70**, 4211 (1991).
[20] G. Napoli, Europhys. Lett. **92**, 46006 (2010).
[21] G. Pampolini and N. Triantafyllidis (unpublished).
[22] J. Nehring, J. Chem. Phys. **56**, 5527 (1972).
[23] W. H. De Jeu, W. A. P. Claassen, and A. M. J. Spruijt, Mol. Cryst. Liq. Cryst. **37**, 269 (1976).
[24] M. Bradshaw, E. Raynes, J. Bunning, and T. Faber, J. Phys. **46**, 1513 (1985).
[25] I. Haller, J. Chem. Phys. **57**, 1400 (1972).
[26] J. Bunning, T. Faber, and P. Sherrell, J. Phys. **42**, 1175 (1981).
[27] J. L. Ericksen, Phys. Fluids (1958-1988) **9**, 1205 (1966).
[28] R. A. Toupin, Arch. Ration. Mech. Anal. **5**, 849 (1956).